Wavefront sensing based on phase contrast theory and coherent optical processing

Lei Huang(黄磊), Qi Bian(边琪)†, Chenlu Zhou(周晨露),
Tenghao Li(李腾浩), and Mali Gong(巩马理)

Center for Photonics and Electronics, Department of Precision Instruments, Tsinghua University, Beijing 100084, *China*

(Received 21 October 2015; revised manuscript received 6 April 2016; published online 31 May 2016)

A novel wavefront sensing method based on phase contrast theory and coherent optical processing is proposed. The wavefront gradient field in the object plane is modulated into intensity distribution in a gang of patterns, making high-density detection available. By applying the method, we have also designed a wavefront sensor. It consists of a classical coherent optical processing system, a CCD detector array, two pieces of orthogonal composite sinusoidal gratings, and a mechanical structure that can perform real-time linear positioning. The simulation results prove and demonstrate the validity of the method and the sensor in high-precision measurement of the wavefront gradient field.

Keywords: wavefront gradients, composite sinusoidal gratings, phase contrast

PACS: 07.07.Df **DOI:** 10.1088/1674-1056/25/7/070701

1. Introduction

The wavefront sensor is one of the most critical elements in the adaptive optical systems, which can perform real-time measurements of the incident wavefront. Wavefront sensing in most of the adaptive optical systems mainly includes a Shack–Hartmann sensor and shearing interferometer.[1] Moreover, new wavefront sensing techniques have been put forward, such as curvature,[2] pyramid,[3,4] phase contrast,[5–7] etc.

Generally, it is difficult to measure the phase distribution directly. The wavefront slopes, gradients or curvature instead of the phase distribution are detected through almost all of the existing wavefront sensing techniques. Thus reconstruction is required to realize phase retrieval. Some of them modulate the wavefront slopes into displacement distribution of spot array, for example, the classical Shack–Hartmann sensor, while the others produce intensity distribution, such as the shearing interferometer and pyramid sensor.[4]

We describe a wavefront sensing technique, called cross phase contrast sensing (CPCS). It is based on the Zernike phase contrast theory and coherent optical processing, with the wavefront gradients modulated into intensity distribution in a gang of patterns. A wavefront sensor is also designed according to the proposed method.[8–11] The sensor is made up of a 4-f system with two pieces of composite sinusoidal gratings placed orthogonally on the Fourier-transform plane,[4,11] as well as a mechanical structure to perform real-time linear positioning of the gratings. The gang of patterns are generated on the image plane by the gratings. As can be seen in the following analysis, the wavefront gradient field can be easily retrieved from the image patterns.

This paper is presented in the following way. Firstly, the principle of the CPCS wavefront sensing is introduced. Secondly, the structure of the CPCS wavefront sensor is designed. The detailed working principle of the sensor is discussed to prove the feasibility of the design. Then, the numerical simulations are made to demonstrate the abilities of the CPCS sensor. The simulation results are compared to the classical methods as well to obtain a better conclusion. Finally, the whole paper is summed up and the performance of the CPCS sensor is illustrated.

2. Principle of the CPCS wavefront sensing

As depicted in the Zernike phase contrast theory, an optical field u, generally described as $U\exp(\mathrm{i}\phi)$, can be approximated as

$$u = U\exp[\mathrm{i}(\phi+\Delta\phi)] \approx U\exp(\mathrm{i}\phi)(1+\mathrm{i}\Delta\phi), \tag{1}$$

when a small phase shift $\Delta\phi$ happens. The small phase variation can be observed only when a certain method is applied, which provides preferential phase-shifting to one of the components by $\pi/2$ or $3\pi/2$. Consequently, the intensity of the re-imaged optical field is proportional to $1\pm 2\Delta\phi$, depending on whether the real component advances or retreats relative to the imaginary one.

As for CPCS, two duplications of the incident optical field are generated and partially overlapped in a micro displacement along the x axis or the y axis. A small phase difference between the two components is added to each point in the overlapped field. Thus, a similar phenomenon happens as depicted in the Zernike phase contrast theory, which is shown in Fig. 1. Here, $\delta\phi^X$ denotes the small phase differences between the two duplications in each point, which are originally induced by the translation. It is assumed that the amplitude of the in-

†Corresponding author. E-mail: bemyselfbq@163.com

© 2016 Chinese Physical Society and IOP Publishing Ltd

cident optical field stays uniform or varies quite slowly compared with the phase, and thus the variety can be ignored.

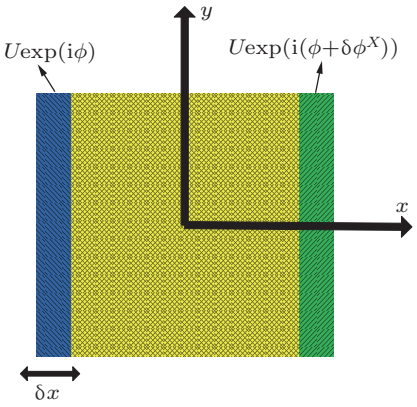


Fig. 1. (color online) The similar phenomenon of CPCS to the phase contrast theory.

Compared with the classical phase contrast techniques, CPCS provides the specific phase shift preferentially to one of the two duplications just before they are added, instead of introducing the additional phase in the overlapped field. Due to this improvement, more flexibility in technique can be accessed as to the custom way. Corresponding to the positive or negative phase contrast respectively, the overlapped field can be described as follows:

$$\begin{aligned} u_{+}^{X} &= U\exp(\mathrm{i}\phi) - \mathrm{i}U\exp\left(\mathrm{i}(\phi+\delta\phi^{X})\right) \\ &= U\exp(\mathrm{i}\phi)\left[(1+\delta\phi^{X}) - \mathrm{i}\right], \qquad (2) \\ u_{-}^{X} &= U\exp(\mathrm{i}\phi) + \mathrm{i}U\exp\left(\mathrm{i}(\phi+\delta\phi^{X})\right) \\ &= U\exp(\mathrm{i}\phi)\left[(1-\delta\phi^{X}) + \mathrm{i}\right]. \qquad (3) \end{aligned}$$

In the equations above, $\delta\phi^{X}$ denotes the small phase differences between the two duplications in each point, which are originally induced by the translation.

Then, we can obtain the corresponding intensity fields as

$$I_{+}^{X} = 2I_{\mathrm{i}}\left(1+\delta\phi^{X}\right), \qquad (4)$$
$$I_{-}^{X} = 2I_{\mathrm{i}}\left(1-\delta\phi^{X}\right), \qquad (5)$$

where I_{i} is the original intensity. Similarly, we can get the intensity fields produced by translation along the y axis

$$I_{+}^{Y} = 2I_{\mathrm{i}}\left(1+\delta\phi^{Y}\right), \qquad (6)$$
$$I_{-}^{Y} = 2I_{\mathrm{i}}\left(1-\delta\phi^{Y}\right). \qquad (7)$$

When all of these four intensity fields are recorded by CCD detector array, the wavefront gradients can be easily calculated according to

$$\frac{\partial\phi}{\partial x} = \frac{1}{\delta x}\frac{I_{+}^{X}-I_{-}^{X}}{I_{+}^{X}+I_{-}^{X}}, \qquad (8)$$
$$\frac{\partial\phi}{\partial y} = \frac{1}{\delta y}\frac{I_{+}^{Y}-I_{-}^{Y}}{I_{+}^{Y}+I_{-}^{Y}}. \qquad (9)$$

All in all, the wavefront gradient field is modulated into intensity distribution in a gang of patterns. As is shown above, only simple calculations are needed to retrieve the wavefront gradients.

3. Design of the CPCS wavefront sensor

Based on the method described above, a CPCS wavefront sensor is proposed.[8–11] The sensor layout is sketched in Fig. 2.

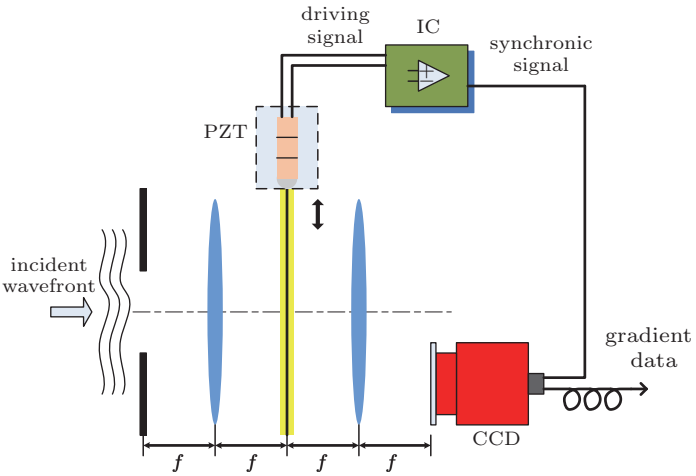


Fig. 2. (color online) The overall layout of the proposed CPCS wavefront sensor.

The main part of the sensor is a 4-f coherent optical processing system with square aperture. The incident wavefront to be detected is located on the object plane, with a square obscure limiting its size. On the Fourier-transform plane, two pieces of composite sinusoidal gratings are inserted.[4,11] They are placed closely to each other and orthogonally along either the x axis or the y axis. By using the gratings, the wavefront gradient field is transformed into intensity distribution in groups of patterns, which can be detected by the detector array on the image plane.

The CCD detector array is placed on the image plane. Since detecting four of the patterns is sufficient to realize gradient measurement, the detector array is set with certain bias beyond the optical axis. As is shown in Fig. 3, the necessary patterns are extracted effectively by using a mask with two rectangular apertures on the image plane.

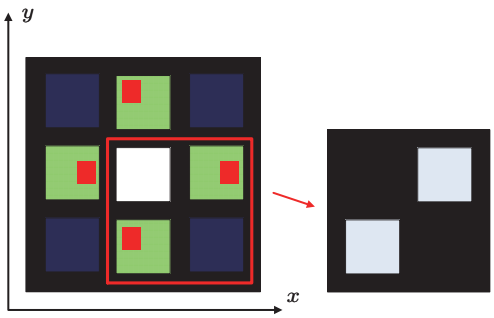


Fig. 3. (color online) The required patterns on the image plane.

Furthermore, the gratings should be placed off axis at a certain distance, so that the phase contrast effect is available. A mechanical structure, which can perform high-precision linear movement, moves the gratings along the diagonal to such a distance. The key component in the mechanical structure is a piezoelectric actuator driven by integrated circuit, which is shown in Fig. 4. As can be seen in the following analysis, when the gratings are moved to a certain distance off the optical axis, the preferential phase shift happens to one of the duplications of the incident optical field. While the gratings are placed on the opposite side, the opposite phase contrast mode can be achieved. In order to synchronize the positioning of the gratings and the snapping of the CCD camera, a synchronizing signal is also needed.

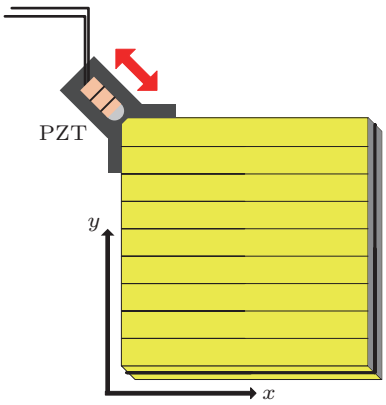


Fig. 4. (color online) A mechanical structure to move the gratings periodically along the diagonal.

To understand how the sensor works, analysis is listed in detail as follows.[8,9] The 4-f system in the sensor realizes two Fourier transforms to the object field through the lens. After being filtered on the Fourier-transform plane, the image field is in the form of a convolution

$$u_{\mathrm{i}}(x_{\mathrm{i}},y_{\mathrm{i}}) = u_{\mathrm{o}}(-x_{\mathrm{i}},-y_{\mathrm{i}}) \otimes T_{\mathrm{s}}(x_{\mathrm{i}},y_{\mathrm{i}}), \tag{10}$$

where u_{o} denotes the object field and T_{s} is the Fourier transform of the complex amplitude transmittance function on the Fourier-transform plane.

Two pieces of composite sinusoidal gratings are inserted orthogonally on the Fourier transform plane of the 4-f system. When the constant factors are ignored, their complex amplitude transmittance function can be written as follows:[10,11]

$$\begin{aligned} t_{\mathrm{s}}^{X}(x_{\mathrm{s}},y_{\mathrm{s}}) &= \frac{1}{2}+\frac{m}{2}(\cos(2\pi f_{\mathrm{g}}x_{\mathrm{s}}) \\ &\quad + \cos[2\pi(f_{\mathrm{g}}+\Delta f_{\mathrm{g}})x_{\mathrm{s}}]), \end{aligned} \tag{11}$$

$$\begin{aligned} t_{\mathrm{s}}^{Y}(x_{\mathrm{s}},y_{\mathrm{s}}) &= \frac{1}{2}+\frac{m}{2}(\cos(2\pi f_{\mathrm{g}}y_{\mathrm{s}}) \\ &\quad + \cos[2\pi(f_{\mathrm{g}}+\Delta f_{\mathrm{g}})y_{\mathrm{s}}]), \end{aligned} \tag{12}$$

where m is the modulus of the transmittance, f_{g} is the basic grating constant, and Δf_{g} stands for the frequency shift, which is much smaller than f_{g}.

Since the two pieces of gratings are placed closely, the total transmittance on the Fourier-transform plane is the product of both

$$t_{\mathrm{s}}(x_{\mathrm{s}},y_{\mathrm{s}}) = t_{\mathrm{s}}^{X}(x_{\mathrm{s}},y_{\mathrm{s}})t_{\mathrm{s}}^{Y}(x_{\mathrm{s}},y_{\mathrm{s}}). \tag{13}$$

Ignoring the additional phase factor, the transmittance function on the image plane becomes

$$T_{\mathrm{s}}(x_{\mathrm{i}},y_{\mathrm{i}}) = \mathrm{FT}[t_{\mathrm{s}}^{X}(x_{\mathrm{s}},y_{\mathrm{s}})] \otimes \mathrm{FT}[t_{\mathrm{s}}^{Y}(x_{\mathrm{s}},y_{\mathrm{s}})]. \tag{14}$$

Its intensity distribution on the image plane can be shown in Fig. 5.

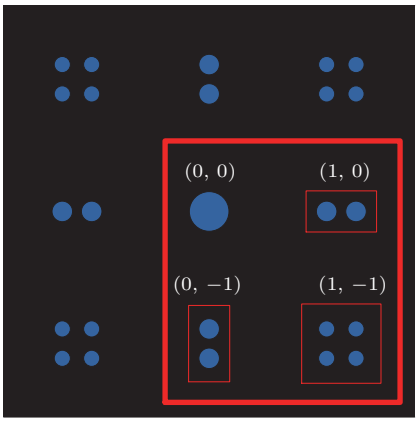


Fig. 5. (color online) Fourier transform of the amplitude transmittance function on the image plane.

In Fig. 5, the blue dots represent the δ sampling function. The gang of patterns divided into nine groups are numbered in the orthogonal coordinates. The transmittance function copies the incident optical field and moves each duplication to the particular location defined by the δ sampling functions. If the grating constant f_{g} is configured appropriately, none of the nine groups will overlap with each other. Considering the configuration in Fig. 3, the patterns lying on the bottom right, with the coordinate (1, 0) and (0, −1), are detected by the CCD camera. When the constant factors are ignored, we can obtain

$$T_{1,0} = \delta(x_{\mathrm{s}} - \lambda f f_{\mathrm{g}}, y_{\mathrm{s}}) + \delta(x_{\mathrm{s}} - \lambda f f_{\mathrm{g}} - \lambda f \Delta f_{\mathrm{g}}, y_{\mathrm{s}}), \tag{15}$$

$$T_{0,-1} = \delta(x_{\mathrm{s}}, y_{\mathrm{s}} + \lambda f f_{\mathrm{g}}) + \delta(x_{\mathrm{s}}, y_{\mathrm{s}} + \lambda f f_{\mathrm{g}} + \lambda f \Delta f_{\mathrm{g}}). \tag{16}$$

The two equations imply that the duplications are separated along the x axis and the y axis respectively, with the same distance

$$\delta x = \delta y = \lambda f f_{\mathrm{g}}, \tag{17}$$

where λ denotes the average wavelength and f is the foci of lens in the 4-f system.

Moreover, moving the gratings along the diagonal in a distance Δd induces additional phase factor between the two duplications, as is shown below

$$\exp(\mathrm{i}2\pi\Delta f_{\mathrm{g}}\Delta d). \tag{18}$$

When the small distance satisfies

$$\Delta d = \pm \frac{1}{4\Delta f_{\mathrm{g}}}, \tag{19}$$

then the additional phase factor turns into $\pm \mathrm{i}$, which corresponds to the positive or negative phase contrast.

With the help of a mechanical structure that can perform real-time linear positioning, the function of moving the gratings along the diagonal can be realized practically. The four intensity fields, i.e., I_{+}^{X}, I_{-}^{X}, I_{+}^{Y}, and I_{-}^{Y}, can be detected almost at the same time. Then the wavefront gradient field can be calculated by using Eqs. (8) and (9). Finally the original wavefront can be reconstructed by the existing algorithm.

4. Simulation and analysis

In order to verify the principle of CPCS, we performed simulations in the MATLAB environment. Incident wavefront with rectangular aperture is generated by using the first 35 orders of Zernike polynomial. The amplitude distribution is assumed to be uniform. The wavefront is then processed in two different ways, i.e., directly differential (which can be seen as the standard way), and detected by the simulations of CPCS. From that we can get the standard wavefront gradients and the CPCS ones. As for further verification, the two gradient fields are reconstructed by Southwell's algorithm[12,13] and the retrieval wavefronts are compared with each other.

The incident wavefront and its Zernike Polynomial coefficients are shown in Fig. 6. Here, the peak and valley (PV) value, as well as the root-mean-square (RMS) value is used to evaluate the wavefront. The PV value represents the maximum of the wavefront distortion and the RMS value describes the degree of the whole wavefront distortion. These two parameters are the most commonly used in practice. As for the Zernike coefficients, the first 35 order Zernike polynomials are usually sufficient to describe the low-frequency aberrations of the high-power lasers.[13]

The groups of patterns are shown in Fig. 7, where both phase contrast modes are presented. The middle pattern, corresponding to $T_{0,0}$ in Part 3, is shielded to make the required patterns apparent. The patterns of (1, 0) and (−1, 0) are related to the gradient field along x axis, while the ones placed at (0, 1) and (0, −1) correspond to the gradient field along y axis. Besides, the patterns with the same coordinate are complementary to each other in opposite phase contrast mode.

Then the patterns located at coordinate (1, 0) and (0, −1) in both phase contrast modes are extracted to calculate the wavefront gradient fields. Actually, taking the patterns on the top and left side will give the same results. In the simulation, some pixels on the edge are also screened, so that the overlapped areas are extracted exactly.

The wavefront gradient fields are shown in Fig. 8, which are generated by CPCS and direct differentiation respectively. As is expected, the wavefront gradient field simulated by CPCS is almost the same as that of direct differentiation.

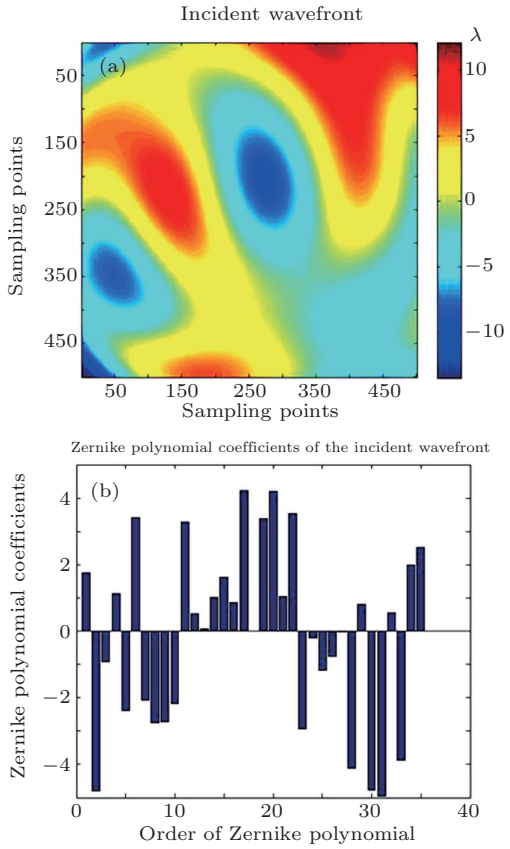


Fig. 6. (color online) (a) The incident wavefront (PV: 25.62λ, RMS: 4.49λ, x scale or y scale: 4 μm/div) and (b) its Zernike polynomial coefficients (order: 1st–35th).

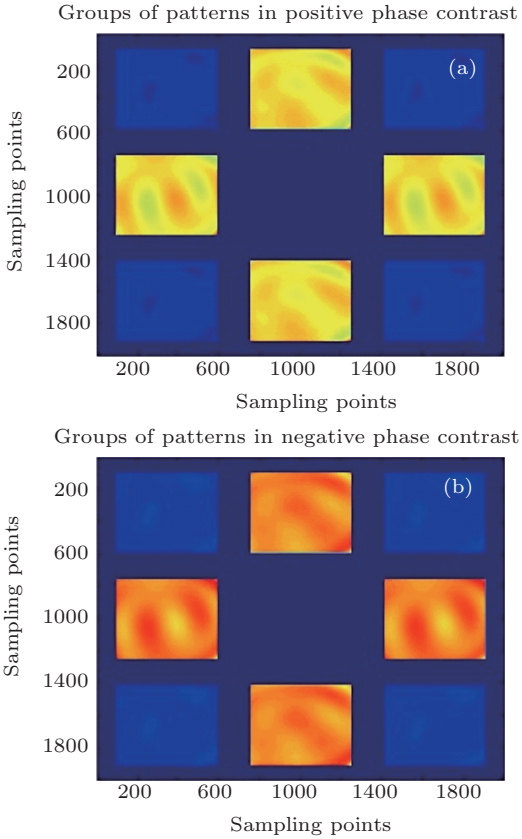


Fig. 7. (color online) Gang of patterns in (a) positive phase contrast and (b) negative phase contrast.

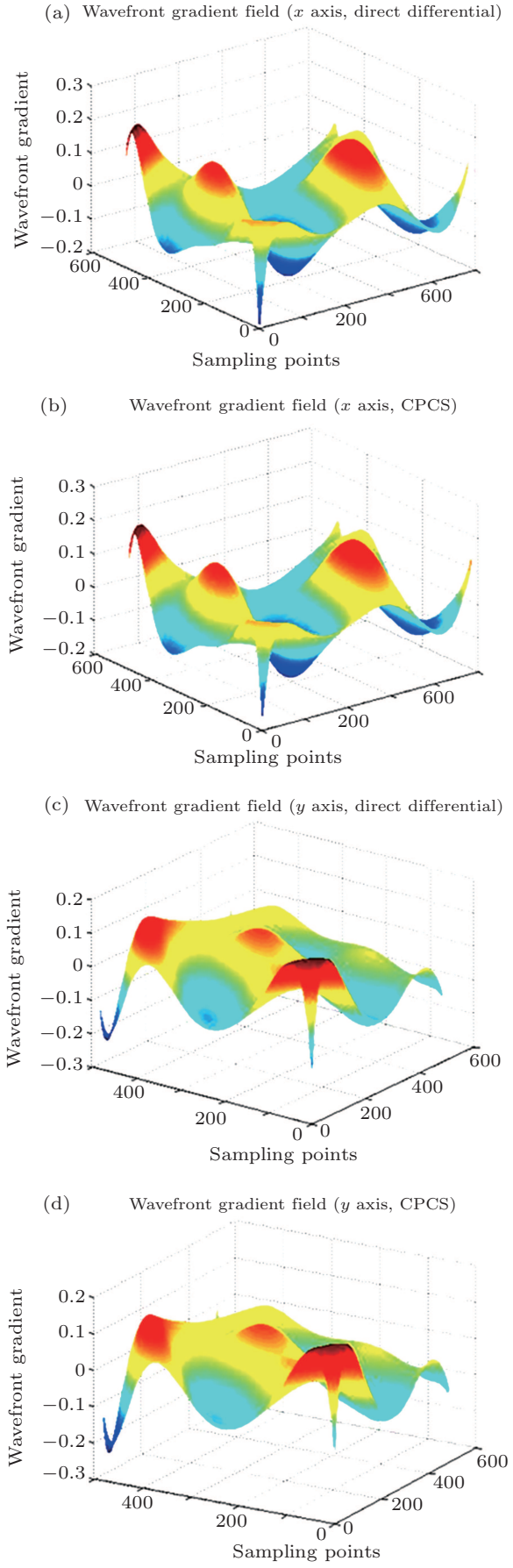


Fig. 8. (color online) The two wavefront gradient fields (a) along x axis, by directly differential, (b) along x axis, by CPCS, (c) along x axis, by directly differential, and (d) along y axis, by CPCS.

Finally, the wavefronts detected through different methods, are retrieved by using the same reconstructor proposed by Southwell. The results are shown in Fig. 9. The wavefront error between CPCS and the standard differential method is 0.12λ in PV and 0.01λ in RMS, while the incident wavefront is a little bit different from the reconstructed ones, which are mainly due to errors of the reconstructor.

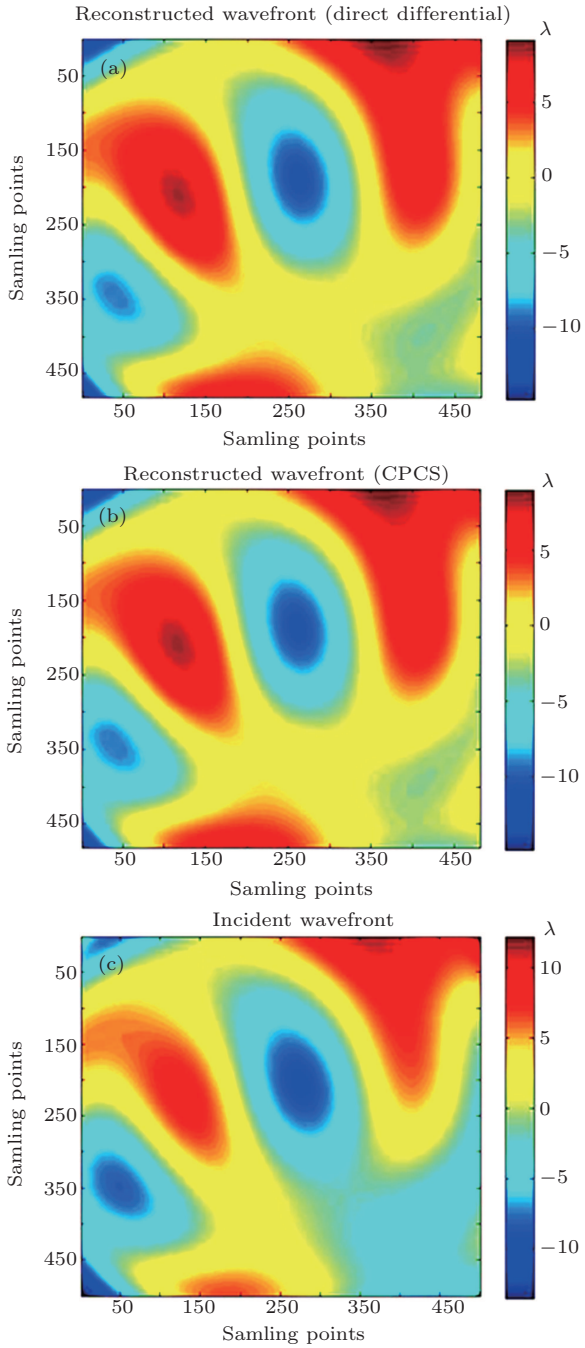


Fig. 9. (color online) The two wavefront retrieved by reconstructor and the incident wavefront. (a) By directly differential (PV: 23.84λ, RMS: 4.36λ, x scale or y scale: 4 μm/div). (b) By CPCS (PV: 23.72λ, RMS: 4.35λ, x scale or y scale: 4 μm/div). (c) The incident wavefront (PV: 25.62λ, RMS: 4.49λ, x scale or y scale: 4 μm/div).

Through the simulation, it can be seen that the proposed sensor is configured in practical parameters. What is more, the

simulation has demonstrated the CPCS detection process and its validity.

On the other hand, CPCS has some characteristics which are quite different from the other wavefront sensors.

In CPCS, wavefront gradient field is modulated into intensity distribution in groups of patterns. As the output intensity distribution is spatially matched with the gradient field in every point, CPCS can perform high-density measurement, which is only limited by the size of the pixels in the detector array. Moreover, CPCS is reference-free, and the calculations have a much smaller complexity than that of the Shack–Hartmann sensor.[14]

Compared with phase-contrast sensing technique,[15–17] CPCS detects gradients rather than directly measures the phase, so that the small phase approximation can be satisfied easily. The way to generate phase contrast effect in CPCS is also quite different from that of phase-contrast sensor. Providing that incident amplitude stays uniform or varies slowly across the object plane, measurement in CPCS is independent with the absolute amplitude of the optical field, which provides the possibilities to gain high precision.

CPCS has much similarity to the lateral shearing interferometer (LSI) and pyramid sensor. For example CPCS also requires that the change of the incident laser intensity must be gentle because the large gradient variation of the intensity causes large errors. However, CPCS has no problem of 2π loss, which is not trivial in LSI.[18] What is more, CPCS is easier to fabricate than the pyramid sensor, for its key components have been commonly used for years.

The dynamic range and resolution of CPCS is mainly limited by the performance of the practical detectors in intensity detection. In fact, the modified phase contrast technique is inherently achromatic. However, the wavefront sensor can perform measurement only with quasi-monochromatic and coherent source, and it limits the sensor's applications. In addition the accuracy of the gratings manufacturing and the piezoelectric actuator translation limits the dynamic range and resolution of CPCS as well.

5. Conclusions

In this paper, a wavefront sensing method CPCS is proposed and a wavefront sensor is also designed by applying the CPCS principles. CPCS is based on the phase contrast theory, while the wavefront sensor uses coherent optical processing to realize the measurement.

In CPCS, the wavefront gradient field is modulated into intensity fields in a gang of patterns. As the output intensity distribution is spatially matched with the gradient field in every point, CPCS can perform high-density measurement, which is only limited by the size of the pixel in the CCD detector array. Besides, CPCS is reference-free and the calibration is not required in use.

In the device, a mechanical structure is implemented to modulate the gratings, with an integrated circuit to synchronize the actuator and the detector. Simulation has demonstrated that the sensing method is valid, and comparisons between CPCS and alternative techniques provide a sight of the novel sensor's interesting characteristics. The calculations have a much smaller complexity than that of the Shack–Hartmann sensor. Compared to the phase contrast sensing technique, CPCS detects wavefront gradients rather than directly measures the phase distribution, so that the small phase approximation can be satisfied easily. In the condition that the incident amplitude stays uniform or varies slowly across the plane, the measurement in CPCS is independent of the absolute amplitude, which provides the possibilities to gain high precision.

For the future work, further study is being made to fabricate CPCS and experiments are being carried out to evaluate its practical performance. Besides, more analysis is needed to model the sensor, as well as new design to improve its ability of broadband measurement.

References

[1] Hardy J W 1998 *Adaptive Optics for Astronomical Telescopes* (Oxford University Press)
[2] Roddier F 1998 *Appl. Opt.* **27** 1223
[3] Ragazzoni R 1996 *J. Mod. Opt.* **43** 289
[4] Wang J X, Bai F Z, Ning Y, Huang L H and Jiang W H 2011 *Acta Phys. Sin.* **60** 025901 (in Chinese)
[5] Bloemhof E E and Wallace J K 2004 *Opt. Express* **12** 6240
[6] Wang Z L, Gao K, Chen J, Ge X, Zhu P P, Tian Y C and Wu Z Y 2012 *Chin. Phys. B* **21** 118703
[7] Du Y, Liu X, Lei Y H, Huang J H, Zhao Z G, Lin D Y, Guo J C, Li J and Niu H B 2016 *Acta Phys. Sin.* **65** 058701 (in Chinese)
[8] Goodman J W 1988 *Introduciton to Fourier Otpics* (2nd Edn.) (Greenwood Village: Roberts and Company Publishers)
[9] Bortz J C 1984 *Opt. Soc. Am. A* **1** 35
[10] Lee S H 1974 *Opt. Eng.* **13** 196
[11] Luo Q, Huang L H, Gu N T and Rao C H 2012 *Chin. Phys. B* **21** 094201
[12] Southwell W H 1980 *J. Opt. Soc. Am.* **70** 998
[13] Xie W K, Gao Q, Ma H T, Wei W J and Jiang W J 2015 *Acta Phys. Sin.* **64** 144201 (in Chinese)
[14] Zhao L P, Guo W J, Li X, and Chen I M 2011 *Opt. Lett.* **36** 2752
[15] Baker K L 2007 *Opt. Express* **15** 5147
[16] Bloemhof E E and Wallace J K 2005 *Proc. SPIE* **5903** 59030Y
[17] Bloemhof E E and Wallace J K 2004 *Proc. SPIE* **5553** 159
[18] Vorontsov M A, Justh E W and Beresnev L A 2000 *Proc. SPIE* **4124** 98